Dynamic Instability Analysis of Internally Damped Rotors

Rim Sino, Eric Chatelet, Olivier Montagnier, Georges Jacquet-Richardet

DYNAMIC INSTABILITY ANALYSIS OF INTERNALLY DAMPED ROTORS

Rim SINO Research Assistant
Eric CHATELET Assistant Professor
Olivier MONTAGNIER† Assistant Professor
Georges JACQUET-RICHARDET Professor

LaMCoS, INSA-Lyon, CNRS UMR5259, F69621, France
E-mail : rim.sino@insa-lyon.fr, eric.chatelet@insa-lyon.fr

Laboratoire de Mécanique et d'Acoustique. UPR CNRS 7051
31 chemin Joseph-Aiguier
13402 Marseille cedex 20 France
E-mail : oliviermontagnier@yahoo.fr

KEYWORDS

Rotordynamics, Internal and External Damping, Stability Criterion, Stability analysis, Threshold speed, Shear effects.

ABSTRACT

This paper deals with the study of dynamic instabilities within rotating assemblies due to internal damping effects. In order to consider realistic mechanical properties, in terms of internal damping, a rheological model is associated to a general finite element beam approach, including transversal shear.
After a description of the theoretical background (choice of internal damping model and equation of motion), an application illustrates the ability of the proposed model. The influence of damping on frequencies and on instability thresholds is investigated using a parametric study. Results are compared to those obtained from an analytical approach as well as from experiments.

1. INTRODUCTION

An accurate modeling of damping characteristics is fundamental in the design of rotating machines for providing an idea about safe speed ranges of rotation. Over the last few years, many studies of rotor dynamic systems have focused on predicting critical speeds, natural frequencies, unbalance responses and, in particular, stability thresholds.

† CReA (Centre de Recherche de l'Armée de l'air), 13300 Salon de Provence, France

Damping is one of the most difficult issues for structural dynamic predictions. The way damping, coming from different sources, shall be considered within a finite element model is not easy. Furthermore, damping is often introduced to control vibrations and designers need methods to optimize the choice of devices or materials providing the proper behavior.

Damping may be classified into the following groups (Osinski (1998)):

- Internal damping associated to all possible ways of energy dissipation related to the internal structure of a vibrating body. It refers to various microscopic phenomena including magnetic effects, thermal effects, and atomic contractions.
- Structural damping. This designation includes energy dissipation occurring at contact surfaces of joints.
- Friction in sliding joints. This can be observed in joint with distinct relative motion, namely in solid bearings, guide poles.
- Hydrodynamic and aerodynamic damping induced by motion of a vibrating structure in a liquid or in a gas.

These damping effects are modeled using two mechanisms: viscous and hysteretic damping. The main difference between both types of damping is that the energy dissipated per cycle by viscous damping is frequency (spin speed) dependent, whereas the energy dissipated by hysteretic damping is not.

Internal viscous damping is well known. Hysteretic damping is often substituted by an equivalent viscous damping for harmonic motions, according eq.(1) within rotating frame (Wettergren (1994)).

$$c_{eq} = \eta k / |\omega - \Omega| \quad (1)$$

where η is the loss factor, ω is the natural frequency, Ω is the speed of rotation, k is the stiffness and c_{eq} is the viscous equivalent damping.

All damping types associated to the non-rotating parts of the structure have a usual stabilizing effect. On the other hand damping associated to rotating parts can trigger instability in supercritical ranges.

The study of spinning shafts with internal damping was first investigated by Newkirk (1924). Although he observed that rotor-disk systems would experience violent whirling at the first natural frequency at speeds above the first critical speed. Kimball (1925) showed that internal damping destabilizes the whirling motion when the rotation speed of the rotor exceeds the first critical speed. Since then, many researchers have studied the influence of internal damping (material, dry friction) as well as external damping (different kind of bearings, squeeze-film, etc.) on the stability of rotating structures. Chatelet (2002), Mazzei (2003) used an analytical method to study the combined effects of internal damping and external damping. Classical results for steel rotors were obtained, showing that rotor stability is improved by increasing the damping provides by the bearings, whereas increasing internal damping may reduce the instability threshold. However, most of this research deals with metallic rotating structures and studies remain purely numerical.

Ehrich (1964), Forrai (1996, 2000) and Nelson (2000) performed a sensitivity analysis from a finite element modeling. They proved that the stability threshold speed coincides with the first forward critical speed regardless of the magnitude of internal damping. They noted that the rotational speed at which the rotor becomes unstable is governed by the ratio of internal and external damping. Addition of external damping can raise the threshold at which the motion will become unstable.

$$\Omega_{th} = \Omega_{cr,1}(1 + \frac{c_e}{c_i}) \quad (2)$$

where c_e is external damping, c_i internal damping, Ω_{th} is the instability threshold and $\Omega_{cr,1}$ the first critical speed.

Chen (1990) and Ku (1998) presented a finite element analysis including combined effects of transverse shear deformation and internal viscous and hysteretic damping. They concluded from a numerical application that hysteretic internal damping leads to the destabilization of forward modes at all spin speeds, whereas viscous internal damping results to the destabilization of forward modes only when the spin speed becomes higher than the critical speed. Backward modes are always stable whatever the amount of internal damping. The same conclusion was given by Melanson (1998) who shows that internal hysteretic damping has always destabilizing effects at every speed. These conclusions were discussed by Genta (2004) who demonstrated that an error is made when considering, as Dimentberge (1961) and Lund (1974), that hysteretic damping of rotating elements is destabilizing at any speed (even subcritical). Genta writes "the fact that it is impossible that any form of rotating damping (including hysteretic damping) is destabilizing in the whole speed range can be shown by a simple reasoning: when the speed tends to zero, the rotor becomes a stationary structure, and damping cannot trigger any form of instability or, with a different phrasing, at very low speed there is not enough energy to sustain vibration, particularly in the presence of energy dissipation due to internal (hysteretic) damping".

In this paper a theoretical background of rotordynamics is first outlined and a finite element beam model is developed for the study of whirl speeds and stability of rotor-bearing systems. In addition to gyroscopic effects, the combined effects of transversal shear and internal damping are considered in order to determine all the elementary matrices associated to the beam element. Finally, an application, including both numerical and experimental results, is provided to illustrate the proposed model and explain the instability of coupled system due to internal damping.

2. FINITE ELEMENT MODEL AND EQUATIONS OF MOTION

Let's consider a spinning uniform beam in a fixed frame as shown in Figure 1.

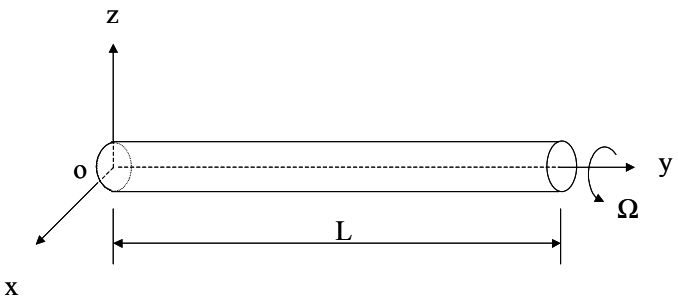

Figure 1: A spinning beam in its fixe frame

2.1 Finite Element Model and Equations Of Motion

Lagrange's equations are used for the derivation of the equations of motion, which can be expressed for a system with non-conservative forces as follows(Lalanne (1998)):

$$\frac{d}{dt}(\frac{\partial T}{\partial \dot{d}_i}) - \frac{\partial T}{\partial d_i} + \frac{\partial U}{\partial d_i} = Fd_i \quad (3)$$

where T and U are the kinetic and potential energies respectively, Fd_i is the generalized forces vector, N

$(1 \le i \le N)$ the number of degrees of freedom and d_i are the generalized independent coordinates. The expression for kinetic energy is:

$$T = \frac{1}{2}\int_0^l \left\{ \begin{array}{l} \rho S\left[\left(\frac{\partial u}{\partial t}\right)^2 + \left(\frac{\partial w}{\partial t}\right)^2\right] \\ +\rho I\left[\left(\frac{\partial \psi}{\partial t}\right)^2 + \left(\frac{\partial \theta}{\partial t}\right)^2\right] + \Omega J\left[\psi\frac{\partial \theta}{\partial t} - \theta\frac{\partial \psi}{\partial t}\right] \end{array} \right\} dy \quad (4)$$

where ρ is the mass density, S the cross-sectional area, I the transverse moment of inertia, J the polar moment of inertia, Ω the rotational speed, l the length of the beam, u and w respectively the transverse deflections in the ox and oz direction while ψ and θ are the corresponding bending angles.

The general expression for the strain energy of the shaft in bending is:

$$U = \frac{1}{2}\int_V \left\{ \varepsilon \right\}^t \left[\sigma \right] .dV \quad (5)$$

Stress and strain are related via the rheological model of Kelvin-Voigt adapted to linear viscoelastic solids. The standard linear model is given by the following relationships between the stress σ et the strain ε which can be split into elastic stress (classical Hooke's law) and dissipative stress function of the speed of deformation (Nashif (1985)):

$$\sigma = E\varepsilon + E\beta\dot{\varepsilon} \quad (6)$$

where E is the Young's elastic modulus et β represents the mechanical damping characteristic of material. The above relation can be written in with transverse shear stresses as following:

$$\tau = G\gamma + G\beta\dot{\gamma} \quad (7)$$

where G the shear modulus, τ the shear stress, γ the shear strain.

The continuous displacement field at material point B on the rotor cross-section without warping function (Figure 2) can be written as follows:

$$\{u(x,y,z)\} = \left\{ \begin{array}{c} u_x(x,y,z) = u(y) \\ u_y(x,y,z) = -z\theta(y) + x\psi(y) \\ u_z(x,y,z) = w(y) \end{array} \right. \quad (8)$$

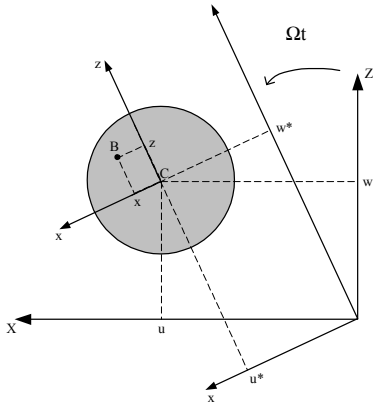

Figure 2:Coordinate of the geometric center and arbitrary point B on the shaft

Hence, the deformation field has the following form:

$$\{\varepsilon\} = \left\{ \begin{array}{c} \varepsilon_{yy} = -z\frac{\partial \theta}{\partial y} + x\frac{\partial \psi}{\partial y} \\ \gamma_{yz} = -\theta + \frac{\partial w}{\partial y} \\ \gamma_{yx} = \psi + \frac{\partial u}{\partial y} \end{array} \right. \quad (9)$$

Beam theory assumes that $\sigma_{xx}=\sigma_{zz}=\sigma_{xz}=0$. Hence, the stress-strain relation can be written as follows:

$$\left\{\sigma\right\} = \left\{ \begin{array}{l} \sigma_{yy} = E_y\varepsilon_{yy} + E_y\beta\dot{\varepsilon}_{yy} \\ \tau_{yz} = G_{yz}\gamma_{yz} + G_{yz}\beta\dot{\gamma}_{yz} \\ \tau_{yx} = G_{yx}\gamma_{yx} + G_{yx}\beta\dot{\gamma}_{yx} \end{array} \right. \quad (10)$$

where, E_y, G_{yz} and G_{yx} are respectively the Young's modulus and transversal shear moduli, and $E_y\beta$, $G_{yz}\beta$ and $G_{yx}\beta$ are respectively the damped Young's modulus and damped transversal shear moduli according to the rotor axis y.

Then the stress vector can be split into elastic stress $\{\sigma\}_e$ and dissipative stress $\{\sigma^*\}_d$:

$$\left\{\sigma\right\} = \left\{\sigma\right\}_e + \left\{\sigma^*\right\}_d \quad (11)$$

Using equation (9), the two parts of equation (11) can be written as follows:

$$\left\{\sigma\right\}_e = \begin{cases} \sigma_{yy} = E_y(-z\dfrac{\partial\theta}{\partial y} + x\dfrac{\partial\psi}{\partial y}) \\ \tau_{yz} = G_{yz}(-\theta + \dfrac{\partial w}{\partial y}) \\ \tau_{yx} = G_{yx}(\psi + \dfrac{\partial u}{\partial y}) \end{cases} \tag{12}$$

$$\left\{\sigma^*\right\}_d = \begin{cases} \sigma_{yy}{}^* = E_y\beta(-z\dfrac{\partial\dot{\theta}}{\partial y} + x\dfrac{\partial\dot{\psi}}{\partial y}) \\ \tau_{yz}{}^* = G_{yz}\beta(-\dot{\theta} + \dfrac{\partial\dot{w}}{\partial y}) \\ \tau_{yx}{}^* = G_{yx}\beta(\dot{\psi} + \dfrac{\partial\dot{u}}{\partial y}) \end{cases} \tag{13}$$

where σ_{yy} and σ^*_{yy} are the normal cross-section stresses, τ_{yz} , τ^*_{yz} and τ_{xy} , τ^*_{xy} are the transversal shear stresses.
Using the equation (5), the elastic energy of the rotor is:

$$U = \frac{1}{2}\int_0^L\int_S \left(\sigma_{yy}\varepsilon_{yy} + \tau_{yz}\gamma_{yz} + \tau_{yx}\gamma_{yx}\right)dSdy \tag{14}$$

The virtual dissipative work due to internal dissipation has the following expression:

$$\delta W = \int_0^L\int_S \left(\sigma^*_{yy}\delta\varepsilon_{yy} + \tau^*_{yz}\delta\gamma_{yz} + \tau^*_{yx}\delta\gamma_{yx}\right)dSdy \tag{15}$$

Then equation (14) can be explicitly written as a function of the displacement field components (equations (9) and (12)):

$$\begin{aligned} U = {} & \frac{1}{2}\int_0^l\int_S E_y\left(z^2(\frac{\partial\theta}{\partial y})^2 + x^2(\frac{\partial\psi}{\partial y})^2\right)dSdy + \\ & \frac{1}{2}\int_0^l\int_S\left[G_{yz}\left(-\psi + \frac{\partial w}{\partial y}\right)^2 + G_{yx}\left(\psi + \frac{\partial u}{\partial y}\right)^2\right]dSdy \end{aligned} \tag{16}$$

The virtual work may also be expressed as a function of the displacement field components using equations (9) and (13).

$$\begin{aligned} \delta W = {} & \int_0^L\int_S E_y\beta\dot{\varepsilon}_{yy}\delta\varepsilon_{yy}dSdy \\ & + \int_0^L\int_S \left(G_{yz}\beta\dot{\gamma}_{yz} + G_{yx}\beta\dot{\gamma}_{yx}\right)\delta\gamma dSdy \end{aligned} \tag{17}$$

which can be written explicitly as follows:

$$\begin{aligned} \delta W = {} & \int_0^L\int_S E_y\beta\left(-z\frac{\partial\dot{\theta}}{\partial y} + x\frac{\partial\dot{\psi}}{\partial y}\right)\left(-z\frac{\partial\delta\theta}{\partial y} + x\frac{\partial\delta\psi}{\partial y}\right)dsdy \\ & + \int_0^L\int_S\left[G_{yz}\beta\left(-\dot{\theta} + \frac{\partial\dot{w}}{\partial y}\right)\left(-\delta\theta + \frac{\partial\delta w}{\partial y}\right)\right]dSdy \\ & + \int_0^l\int_S\left[G_{yx}\beta\left(\dot{\psi} + \frac{\partial\dot{u}}{\partial y}\right)\left(\delta\psi + \frac{\partial\delta u}{\partial y}\right)\right]dsdy \end{aligned} \tag{18}$$

The application of Lagrange's equations to the kinetic energy, potential energy and virtual work, leads to the following equation of motion in the fixed frame:

$$\begin{aligned} & [M]\left\{\ddot{d}\right\} + [C_i + C(\Omega)]\left\{\dot{d}\right\} \\ & + [K + K_i(\Omega)]\{d\} = \{F(t)\} \end{aligned} \tag{19}$$

where $[M]$ is the symmetric mass matrix, $[C(\Omega)]$ the global asymmetric matrix including an antisymmetric gyroscopic matrix (function of Ω speed of rotation) and a frequently asymmetric matrix owing to the characteristics of bearing, $[K]$ is the elastic stiffness matrix that is frequently asymmetric owing to the characteristics of bearings, $[C_i]$ and $[K_i(\Omega)]$ are respectively the internal damping matrix and the stiffness matrix (function of the rotation speed) associated to internal damping β. $\{F(t)\}$ is the generalized force vector and $\left[\ddot{d}\right]$, $\left[\dot{d}\right]$ and $\left[d\right]$ are respectively the nodal acceleration, velocity and displacement. The associated elementary matrices, mass stiffness gyroscopic and internal damping, are given in appendix A.

The Campbell diagram (evolution of natural frequency as a function of rotational speed) and stability regions are then determined from the solution of the eigenvalue problem obtained after reduction by the pseudo modal method (Lalanne (1998)).

$$\{d\} = [\phi]\{p\} \tag{20}$$

where $[\phi]$ is constituted by the mode shapes of the conservative system at rest (Ω=0), $\{p\}$ are the generalized modal coordinates.

Then, equation (19) is written under following relation:

$$[m]\{\ddot{p}\} + [c_i + c(\Omega)]\{\dot{p}\} + [k_i(\Omega) + k]\{p\} = \{f(t)\} \tag{21}$$

with [m], [c] and [k] are the classical generalized modal matrices. As all elements of the finite element model are supposed to have the same material properties, they are characterized by the same internal damping

In order to determine the internal damping matrices, it is necessary to estimate the mechanical damping characteristic β. Here, classically, this parameter is obtained from the material hysteretic damping η, known experimentally under harmonic

motion. Hysteretic damping is then transformed into an internal equivalent viscous damping as shown in equation (1). Such transformation is frequency dependent.

3. VALIDATION-EXPERIMENTAL AND NUMERICAL APPLICATIONS

In order to illustrate the influence of internal and external damping within rotordynamic analyses, instability thresholds are determined from an experimental set up developed at the LMA of Marseille, France Montagnier (2005).
The experimental device shown in Figure 3 is used to study the stability of shafts made of different materials.

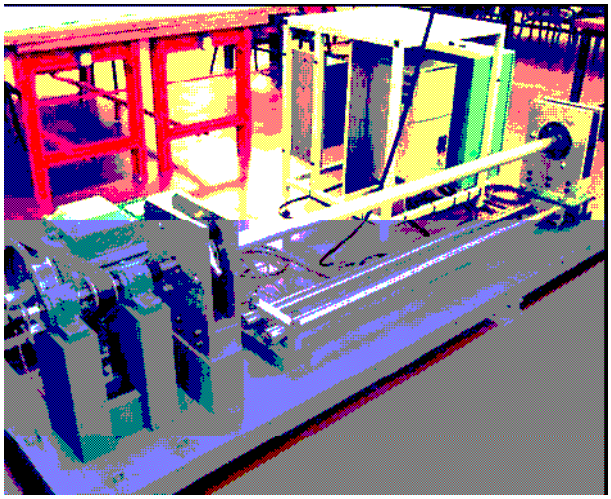

Figure 3: Testing machine for high- speed tubes

To allow supercritical behavior, it is necessary to introduce external damping. Passive dissipation is introduced at bearing levels with viscoelastic supports (Figure 4). Bearings are classical ball bearings. Viscoelastic support work in shear to obtain symmetric behavior. The bearing characteristics are presented in table 1 and table 2.

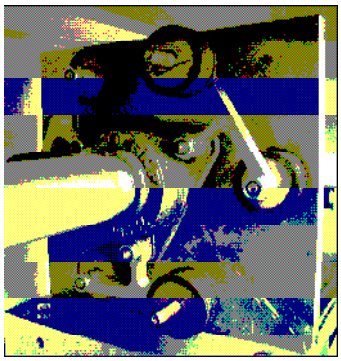

Figure 4: Viscoelastic support (natural rubber)

A hollow shaft model supported by two bearings at the ends is considered as shown in Figure 5 (Montagnier and Hochard (2005)):

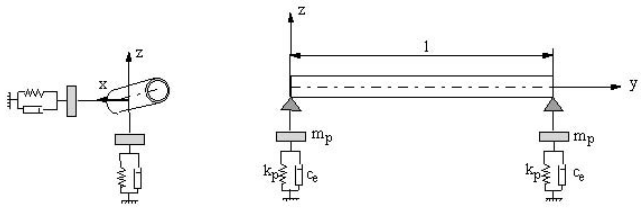

Figure 5: Rotor model

The equivalent internal viscous damping is given by term c_i. Viscoelastic supports (Figure 5) are supposed to be symmetric (same stiffness and damping in all directions in *Oxz* plane). The viscoelastic model consists of a stiffness k_p and a viscous damping c_e. Bearings are supposed to be infinitely rigid (mass m_p). The material properties and the isotropic bearing stiffness and damping characteristics of the Aluminum and PVC rotors considered are summarized in Table 1 and Table 2. These values were estimated directly from a high-speed rotor test bench.

Instability is studied for both Aluminum and PVC tubes via parametric study of the bearing-shaft system. Various lengths, ranging between 0.5m and 3m are considered for the Aluminum tube and between 0.4m and 1.4m for the PVC tube. They are characterized by a low stiffness and a high damping. These characteristics tend to decrease the instability threshold.

The values of external damping (viscous damping c_e = 100 N/m/s) are given by a damping factor ξ_e = 3.5% whereas the values for internal damping are introduced in the FE program and relation $\eta_i=2\xi_i$, with ξ_i characterized in Tables 1 and 2. Solution of the equation of motion (eq. 21) gives the frequencies of the coupled system as well as the instability thresholds of the associated modes.

Table 1: Data of Aluminum rotor.

Young modulus	E	GPa	69
Mass density	ρ	kg/m^3	2700
Length of tube	L	m	1.64
External radius	R_e	m	0.025
Internal radius	R_i	m	0.02298
Internal damping factor	ξ_i	%	0.2
External damping factor	ξ_e	%	3.5
Bearing Mass	m_p	kg	2.817
Support Rigidity	K_p	N/m	564.10^3

Table 2: Data of PVC rotor

Young modulus	E	GPa	2.2
Mass density	ρ	kg/m^3	1350
External radius	R_e	m	0.025
Internal radius	R_i	m	0.0215
Internal damping factor	ξ_i	%	1.25
External damping factor	ξ_e	%	3.5
Bearing Mass	m_p	kg	2.608
Support Rigidity	K	N/m	567.10^3

Parametrical studies are performed on the Aluminum and PVC rotors

Figure 6 and Figure 7 show respectively the evolution of frequencies of the system as well as instability thresholds, with respect to the length of the rotor L. Legends are as follows: F_{csi} represents the i^{th} frequency of the coupled system; SI_i represents the i^{th} associated instability threshold.

Internal damping induces the destabilization of forward modes, only when the spin speed becomes higher than the critical speed. Backward modes are always stable (see appendix B)

When comparing these instability cards, it appears that the instability zone (grey) of the Aluminum rotor is smaller than the stability zone of the PVC rotor. The difference is due to the internal material damping ξ_i which is more important for PVC than for Aluminum (see Table 1 and Table 2).

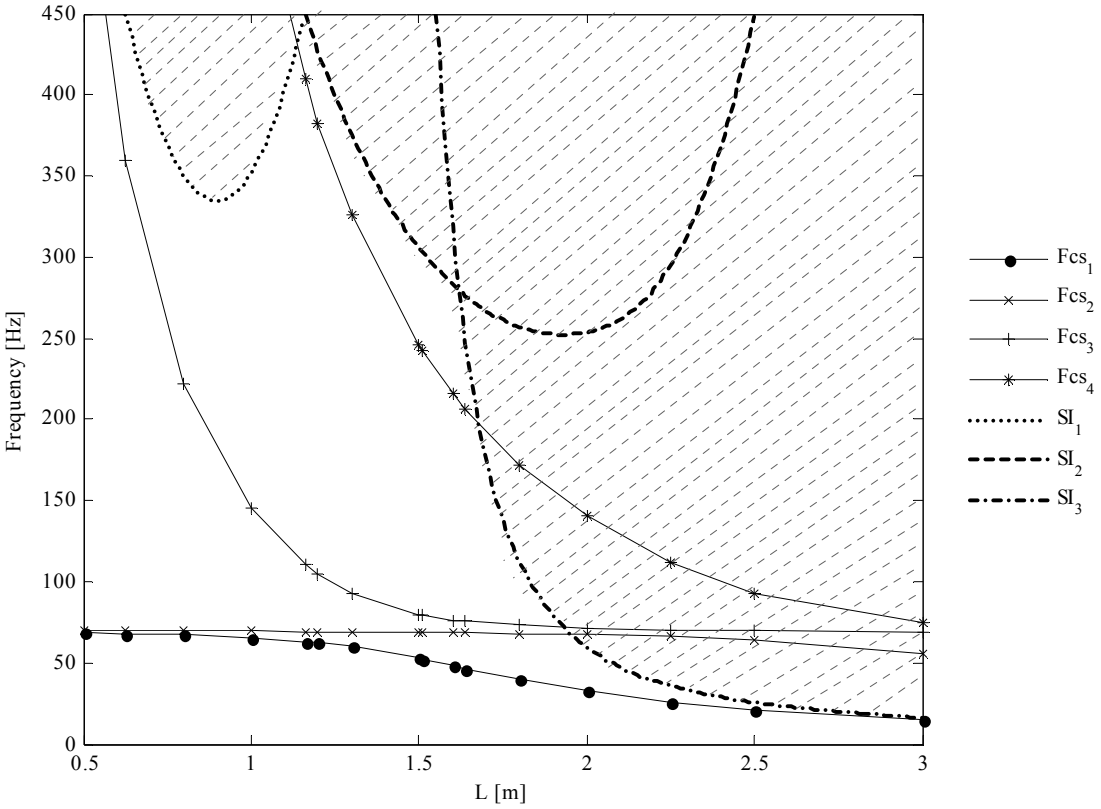

Figure 6: Frequencies and instability thresholds for Aluminum Tube

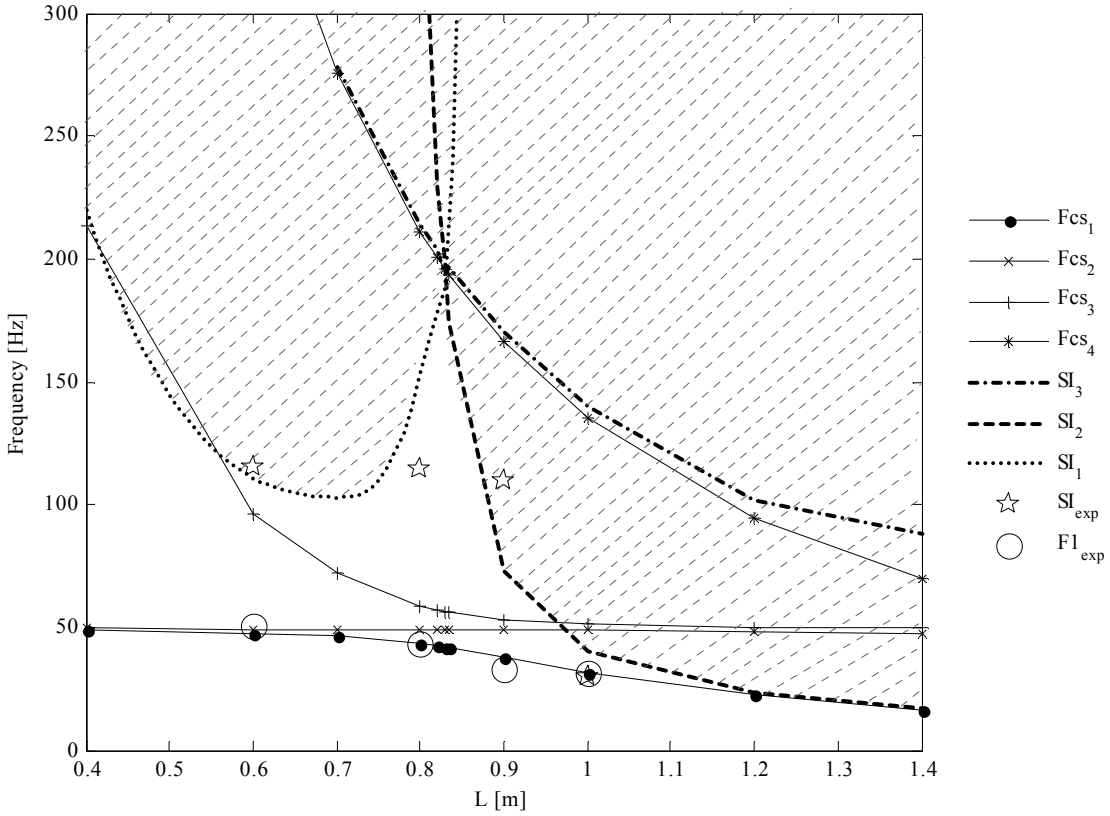

Figure 7: Frequencies and instability thresholds of PVC Tube: numeric and experimental.

Experimental results obtained at the LMA are plotted in Figure 7 too. They are symbolized by a "circle ○" for the first experimental frequency and by a "star ☆" for the associated instability thresholds. Four experimental tests were performed for PVC tubes of lengths 0.6m, 0.8m, 0.9m and 1m. The experimental instability was detected at the first critical speed. Tendencies shown by experimental results are in good agreement with theoretical results and the first frequency identified matches very well.

The observation of Figure 7 also shows two instability zones merging at a length L near 1.44m for Aluminum tube and 0.8m for PVC. In fact, this zone corresponds to the zone where the system is the most coupled (flexible tube on flexible foundations). Coupling of the system is quantified by comparing the frequency of the flexible rotor mounted on rigid bearings (noted Ω_1) with the frequency of the rigid rotor mounted on flexible bearings (noted ω_{01}). An increase of the zone of stability is also observed at this point where those frequencies are equal.

The frequencies associated to the rigid rotor may be estimated from the following relation (Montagnier (2005)):

$$\omega_{0n} = \sqrt{\frac{k_p}{m_p + \frac{m_a}{2(2+(-1)^n)}}} \tag{22}$$

where k_p is the bearing stiffness, m_a the mass of the tube and n the mode number. These two first frequencies are denoted in the following F_{rr1} and F_{rr2} (frequencies of rigid rotor with flexible bearings).

The frequencies of the tube supported by rigid bearings may be estimated from the well known analytical equation:

$$\Omega_n = \left(\frac{\pi n}{l}\right)^2 \sqrt{\frac{EI}{\rho S}} \tag{23}$$

Where E is the Young's modulus, I the area moment of inertia of the beam cross-section about the neutral axis y, ρ is the mass per unit volume, l the length of rotor, S the cross-sectional area of the beam and n is the mode number, with $1 \le n \le N$. The first two frequencies are denoted in the following F_{rb1} and F_{rb2} (frequencies with rigid bearings and flexible rotor).

When zooming the coupling zone (Figure 8 and Figure 9), a significant evolution is observed for the resulting natural frequencies of the coupled system.

The evolution of frequency and instability thresholds associated to the mostly coupled system are explained as follows. For this particular length of rotor, bearings are highly responding and then provide more external damping to the system, increasing stability.

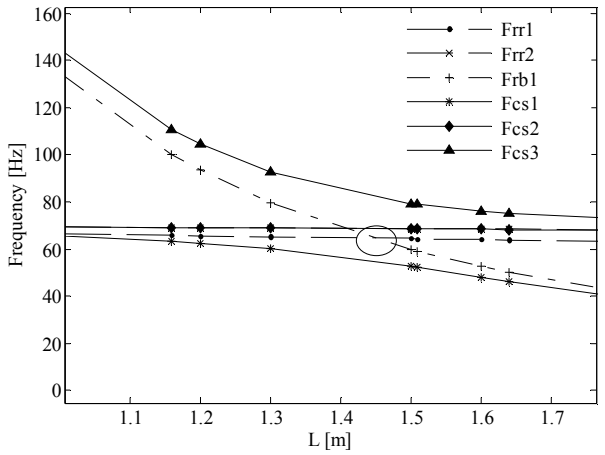

Figure 8: Zoom of coupling zone of coupled and uncoupled systems for Aluminum Tube

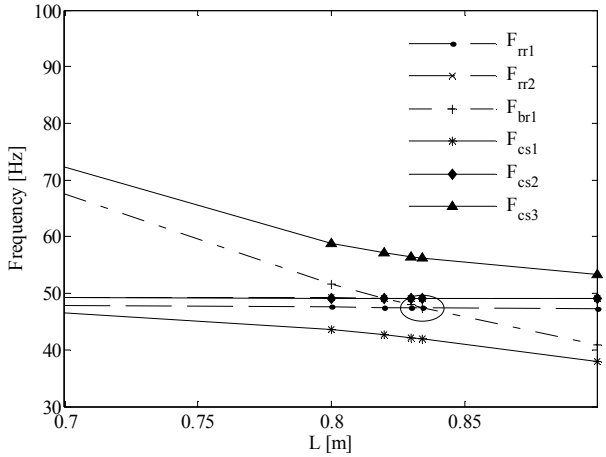

Figure 9: Zoom of coupling zone of coupled and uncoupled systems for PVC Tube

Such behavior has also been observed by Dutt (1992) who shows that a proper selection of the value of support parameters can increase significantly instability threshold for a system on viscoelastic supports. Viscoelastically damped support gives the highest values of instability threshold compared with either viscously or elastic supports.

4. CONCLUSION

This work deals with the stability analysis of an internally damped rotating shaft. A modeling based on a Finite Element method considers internal damping using a Kelvin-Voigt rheological model. An experimental bench is used for the validation of the method.

A parametrical analysis demonstrates the influence of internal/external damping on frequencies and instability thresholds for a coupled system.

Validation is achieved from a PVC material tube.

The developed method and associated experimental test bench shall now be used to study the dynamic stability of composite rotors for different configurations of wall thickness.

REFERENCES

[1] Osinski Z., 1998, “Damping of vibrations, institute of machine design fundamentals”, Warsaw university of technology, Warsaw, Poland. A.A.BALKEMA/ ROTTERDAM/BROOKFIELD.

[2] Wettergren H.L., 1994, “Dynamic Instability of Composite Rotors”, IFToMM Fourth International Conference on Rotor Dynamics, Chicago Illinois 7-9 September, pp287-292.

[3] Newkirk B.L., 1924, “Shaft Whipping», General Electric Review, vol. 27(3), pp. 169-178.

[4] Kimball A.L., 1925, ”Internal friction as a cause of shaft whirling”, Philosophical Magazine, Series 6, vol. 49(1), pp. 724.

[5] Chatelet E., Lornage D. and Jacquet-Richardet G., 2002, “A three-dimensional modeling of the dynamic behavior of composite rotors”, International Journal for Rotating Machinery, vol. 8(3), pp. 185-192.

[6] Mazzei, A.J. and Scott, R.A., 2003, “Effects of Internal Damping on the Stability of a Rotating Shaft Driven through a Universal Joint”, Journal of sound and vibration. Vol. 265, pp. 863-885

[7] Ehrich F.F., 1964, “Shaft Whirl Induced by Rotor Internal Damping”, Journal of Applied Mechanics, ASME, vol. 31, pp279-282.

[8] Forraï L., 1996, “Stability Analysis of Symmetrical Rotor-Bearing Systems With Internal Damping Using Finite Elements Method”, *International Gas Turbine and Aeroengine Congress and Exhibition,* UK, ASME Paper N° 96-GT-407.

[9] Forraï L., 2000, “A finite Elements Model for Stability Analysis of Symmetrical Rotor Systems With Internal Damping”, Journal of Computational and Applied Mechanics, Vol. 1 pp 37-47.

[9] Cerminaro A.M. and Nelson F.C, 2000, “The effect of Viscous and hysteretic Damping rotor stability”, ASME TURBOEXPO 2000, May 8–11, Munich, Germany.

[10] Chen L.-W. and D. -M. Ku, 1990, “Dynamic Stability Analysis of a Rotating Shaft by the Finite Element Method», Journal of Sound and Vibration, Vol. 143,N° 1, pp. 143-151.

[11] Ku D. -M., 1998, "Finite element analysis of whirl speeds for rotor-bearing systems with internal damping", mechanical systems and signal processing, 12(5, 599-610).
[12] Melanson J. and Zu J.W., 1998, "Free Vibration and Stability Analysis of Internally Damped Rotating Shafts With General Boundary Conditions", Journal of Vibration and Acoustics, Transactions of the ASME, vol. 120, pp 776-783.
[13] Genta G., 2004, "On a persistent Misunderstanding of the role of Hysteretic Damping in Rotordynamics", Journal of Vibration and Acoustics, Vol. 126, pp. 459-461.
[14] Dimentberg M., 1961, "Flextural Vibration of Rotating Shafts", Butterworth, London, England.
[15] Lund J. W., 1974, "Stability and Damped Critical Speeds of Flexible Rotor in Fluid Film Bearings", ASME J. IND.,96, pp.509-517.
[16] Lalanne M., Ferraris G., 1998, "Rotordynamics Prediction in Engineering", 2nd edition, J. Wiley and Sons, 254 p.
[17] Montagnier O et Hochard C., 2005, "Etude théorique et expérimentale de la Dynamique des arbres de transmission supercritiques", 17ème congrès Français de Mécanique, Troyes, 29 Août-2 Septembre 2005.
[18] Montagnier O. et Hochard C.,"design of supercritical composite helicopter driveshafts: theoretical and experimental study.", european conference for aerospace sciences (EUCASS). 2005
[19] Dutt J.K. et Nakra B.C.,1992 "Stability of rotor systems with viscoelastic supports", Journal of Sound and Vibration, Vol. 153,N° 1, pp. 89-96.
[20] M. L. Adams, JR., 2001, "Rotating Machinery Vibration", Marcel Dekker, 354 p.

Appendix A:

The shaft is modeled with beam finite elements with two nodes, then eight degrees of freedom, four displacements and four slopes. The nodal displacement vector is:

$$d = \left[u_1, w_1, \theta_1, \psi_1, u_2, w_2, \theta_2, \psi_2\right]^t \tag{24}$$

Mass matrix:

$$\mathbf{M} = \frac{\rho L}{840(1+a)^2}\begin{bmatrix} M_1 & 0 & 0 & M_7 & M_{11} & 0 & 0 & M_{29} \\ & M_1 & -M_7 & 0 & 0 & M_{11} & -M_{29} & 0 \\ & & M_6 & 0 & 0 & M_{29} & M_{24} & 0 \\ & & & M_6 & -M_{29} & 0 & 0 & M_{24} \\ & & & & M_1 & 0 & 0 & -M_7 \\ & & & & & M_1 & M_7 & 0 \\ & & & & & & M_6 & 0 \\ sym & & & & & & & M_6 \end{bmatrix} \tag{25}$$

where

$$\begin{cases} M_1 = S\left(312+588a+280a^2\right)+\dfrac{1008I}{L^2} \\ M_7 = -S\cdot L\left(44+77a+35a^2\right)-\dfrac{\left(84-420a\right)I}{L} \\ M_6 = S\cdot L^2\left(8+14a+7a^2\right)+I\left(112+140a+280a^2\right) \\ M_{11} = S\left(108+252a+140a^2\right)-\dfrac{1008I}{L^2} \\ M_{24} = -S\cdot L^2\left(6+14a+7a^2\right)-I\left(28+140a-140a^2\right) \\ M_{29} = S\cdot L\left(26+63a+35a^2\right)-\dfrac{\left(84-420a\right)I}{L} \end{cases} \tag{26}$$

Gyroscopic matrix:

$$\mathbf{C} = \frac{\rho I}{30L(1+a)^2}\begin{bmatrix} 0 & C_2 & C_4 & 0 & 0 & -C_2 & C_4 & 0 \\ & 0 & 0 & C_4 & C_2 & 0 & 0 & C_4 \\ & & 0 & C_9 & C_4 & 0 & 0 & C_{31} \\ & & & 0 & 0 & C_4 & -C_{31} & 0 \\ & & & & 0 & C_2 & -C_4 & 0 \\ & & & & & 0 & 0 & -C_4 \\ & & & & & & 0 & C_9 \\ anti & sym & & & & & & 0 \end{bmatrix} \tag{27}$$

where

$$\begin{cases} C_2 = -72 \\ C_4 = -L\left(6-30a\right) \\ C_9 = -L^2\left(8+10a+20a^2\right) \\ C_{31} = L^2\left(2+10a-10a^2\right) \end{cases} \tag{28}$$

Stiffness matrix

$$\mathbf{K} = \frac{EI}{(1+a)L^3}\begin{bmatrix} 12 & 0 & 0 & -6L & -12 & 0 & 0 & -6L \\ 0 & 12 & 6L & 0 & 0 & -12 & 6L & 0 \\ 0 & 6L & (4+a)L^2 & 0 & 0 & -6L & (2-a)L^2 & 0 \\ -6L & 0 & 0 & (4+a)L^2 & 6L & 0 & 0 & (2-a)L^2 \\ -12 & 0 & 0 & 6L & 12 & 0 & 0 & 6L \\ 0 & -12 & -6L & 0 & 0 & 12 & -6L & 0 \\ 0 & 6L & (2-a)L^2 & 0 & 0 & -6L & (4+a)L^2 & 0 \\ -6L & 0 & 0 & (2-a)L^2 & 6L & 0 & 0 & (4+a)L^2 \end{bmatrix} \tag{29}$$

where:

$$a = \frac{12EI}{GS_rL^2} \tag{30}$$

Internal damping matrices:

$$\mathbf{C_i} = \frac{EI\beta}{(1+b)L^3}\begin{bmatrix} 12 & 0 & 0 & -6L & -12 & 0 & 0 & -6L \\ & 12 & 6L & 0 & 0 & -12 & 6L & 0 \\ & & (4+b)L^2 & 0 & 0 & -6L & (2-b)L^2 & 0 \\ & & & (4+b)L^2 & 6L & 0 & 0 & (2-b)L^2 \\ & & & & 12 & 0 & 0 & 6L \\ & & & & & 12 & -6L & 0 \\ & & symmetric & & & & (4+b)L^2 & 0 \\ & & & & & & & (4+b)L^2 \end{bmatrix} \quad (31)$$

$$\mathbf{K_i} = \frac{EI\beta}{(1+b)L^3}\begin{bmatrix} 0 & -12 & -6L & 0 & 0 & 12 & -6L & 0 \\ & 0 & 0 & -6L & -12 & 0 & 0 & -6L \\ & & 0 & -(4+b)L^2 & -6L & 0 & 0 & -(2-b)L^2 \\ & & & 0 & 0 & -6L & (2-b)L^2 & 0 \\ & & & & 0 & -12 & 6L & 0 \\ & & & & & 0 & 0 & 6L \\ & & anti-symmetric & & & & 0 & -(4+b)L^2 \\ & & & & & & & 0 \end{bmatrix} \quad (32)$$

where:

$$b = \frac{12EI\beta}{GS_r\beta L^2} \quad (33)$$

Appendix B: Physical rotordynamics instability

As shown in Figure 10, when the rotor spins slower than the orbit natural frequency, rotor internal damping causes an orbital disturbance to decay (stable motion) (Adams 2001).

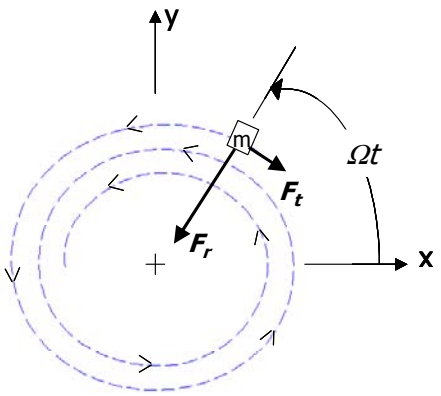

Figure 10: forward precession with Ω<ω

Conversely, when the rotor and its internal damping mechanism rotate faster (at higher frequency) than the orbit natural frequency (Figure 11), the rotor internal damping "pulls" tangentially in the direction of orbiting and thereby imparts energy to the orbital vibration mode, causing the mode to become " self-excited " at its natural frequency (leads to instability).

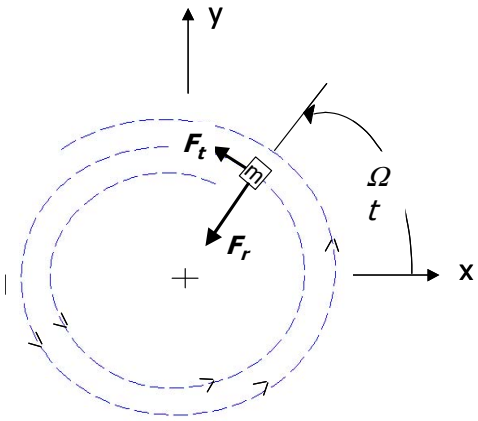

Figure 11: forward precession with Ω>ω

But with backward precession, the speed of the mode is always negative and the internal damping generates a positive tangential force in the opposite direction of the mode speed so that will drag the mode and will decrease the orbit of the motion so the motion is stable (Figure 12).

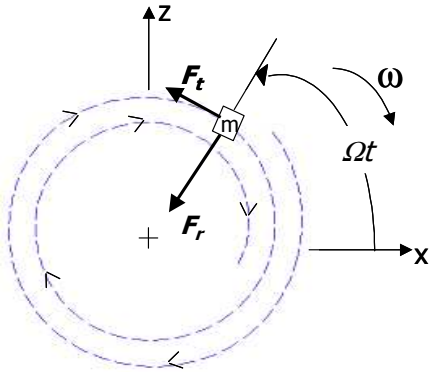

Figure 12: backward precession